Magnetic spiral induced by strong correlations in $MnAu_2$

J. K. Glasbrenner
National Research Council/Naval Research Laboratory, Washington, DC 20375, USA

K. M. Bussmann and I. I. Mazin
Naval Research Laboratory, Washington, DC 20375, USA

(Received 2 July 2014; revised manuscript received 16 September 2014; published 17 October 2014)

The compound $MnAu_2$ is one of the oldest known spin-spiral materials, yet the nature of the spiral state is still not clear. The spiral cannot be explained via relativistic effects due to the short pitch of the spiral and the weakness of the spin-orbit interaction in Mn, and another common mechanism, nesting, is ruled out as direct calculations show no features at the relevant wave vector. We propose that the spiral state is induced by a competition between the short-range antiferromagnetic exchange and a long-range interaction induced by the polarization of Au bands, similar to double exchange. We find that, contrary to earlier reports, the ground state in standard density functional theory is ferromagnetic, i.e., the latter interaction dominates. However, an accounting for Coulomb correlations via a Hubbard U suppresses the Schrieffer-Wolff-type s-d magnetic interaction between Mn and Au faster than the superexchange interaction, favoring a spin-spiral state. For realistic values of U, the resulting spiral wave vector is in close agreement with experiment.

DOI: 10.1103/PhysRevB.90.144421 PACS number(s): 75.10.Hk, 75.10.Lp, 75.25.−j, 75.10.Jm

I. INTRODUCTION

The magnetic spiral is a type of noncollinear magnetic ordering in materials in which the localized moments form a screw-type pattern about an axis. Since the discovery of the first spin spiral in $MnAu_2$ in 1956 [1], the origins of such spirals have been the subject of intensive research. A number of mechanisms have been discussed. In the local-moment Heisenberg-exchange picture, a natural source of spirals is magnetic frustration of the nearest- and next-nearest-neighbor exchange parameters, for example, when $J_1 \neq 0$ (ferro- or antiferromagnetic) and $J_2 > 0$ (antiferromagnetic). If the next-nearest-neighbor exchange is large enough, such that $|J_1| < 4|J_2|$, then the mean-field solution yields a spiral ground state [2,3]. This mechanism is applicable in both localized and itinerant electron systems, although in the latter one may expect long-range interactions to play a role. For an itinerant system, the structure of the electronic response in reciprocal space captures the role of such interactions. If there is a maximum in the spin susceptibility at a particular wave vector $\mathbf{q}$, then this generates a spin-density wave with the same wave vector, which can take the form of a spin spiral. In principle, a kink [as in the uniform two-dimensional (2D) electron gas] or even a derivative singularity (as in the 3D electron gas) can induce an oscillatory interaction [Ruderman-Kittel-Kasuya-Yosida (RKKY) interaction] in real space, which can also encourage a spiral formation. Contrary to a common misconception, this effect does not require electron bands crossing the Fermi surface (the interaction is defined by the real, not imaginary, part of susceptibility), but it does become weaker as the excitation gap grows. Finally, geometric frustration can also encourage noncollinearity and helical ordering in materials.

The Dzyaloshinskii-Moriya (DM) interaction [4,5], a relativistic effect that occurs in materials without an inversion center, has attracted a substantial amount of interest and can lead to moment canting or spiraling. This interaction becomes more important in materials with heavy elements, such as the rare-earth series. Relativistic effects are important in such materials, although more than one mechanism is often in play. For example, the spiral phases of the heavy rare-earth metals Tb-Tm [6] are also understood to be due to nesting [7–9].

Spiral ordering is not restricted to materials with heavy magnetic ions. Spirals also form in lighter transition-metal materials with an intriguing range of spiral vectors $\mathbf{q}$. The DM mechanism may be operative in some of these materials, but in such systems the weak relativistic effects induce spirals with long wavelengths, as in MnSi [10–12]. Shorter wavelength spirals are also common, such as in the magnetically frustrated spinel chromites $ZnCr_2Se_4$ [13] and $CdCr_2O_4$ [14]. An interesting example is FeAs, featuring an incommensurate spiral with a period of 20 Fe layers [15,16]. This material is a good metal, so one may think that the conduction electrons mediate an oscillatory interaction via nesting or the classical 3D RKKY mechanism. However, the search for a nesting vector or features in the noninteracting susceptibility that match the spin-spiral vector was unsuccessful [17]. But, as in the cited example of the 3D electron gas, oscillatory interactions may manifest themselves even without such peaks, and so one cannot rule out this mechanism in total without a full calculation of spin susceptibility in real space.

The material $MnAu_2$, as stated above, is one of the earliest examples of magnetic spiraling [1,18,19] and may provide better clues than FeAs as to how short-period spirals can form. The spiral has an even shorter period than FeAs, the material is a metal, and, unlike FeAs, Mn d states are removed from the Fermi level, so the system may be a better representation of a model with localized moments and an interaction transferred *via* itinerant electrons of a different nature. The magnetic structure consists of ferromagnetic Mn planes (local moments are in-plane) stacked along the crystallographic c axis, with the in-plane magnetization direction rotating from plane to plane, as illustrated in Fig. 1(b). The rotation angle varies with temperature, from 60° at 5 K to 40° at 250 K [20]. The Néel temperature is $T_N = 363$ K [1] and the material transitions from the spiral to a ferrimagnetic fanlike structure

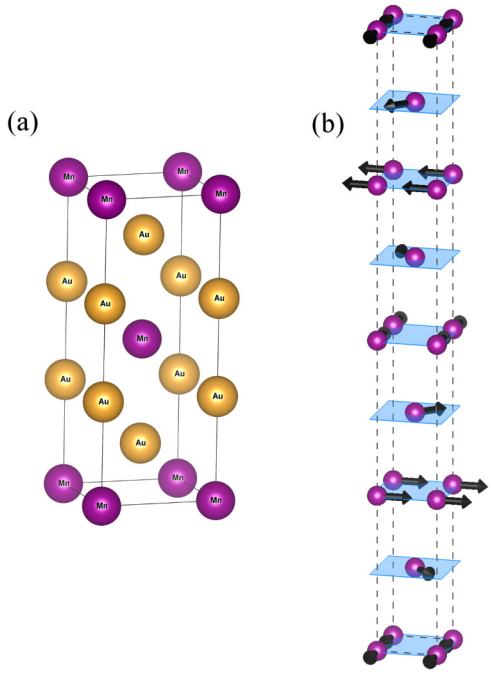

FIG. 1. (Color online) (a) A schematic [21] of the crystal structure of $MnAu_2$. (b) A schematic supercell [21] of a magnetic spiral with $\mathbf{q} = \{0,0,\pi/2c\}$ in $MnAu_2$.

at room temperature upon application of a ∼10 kOe magnetic field [1,18,22], which gives rise to a giant magnetoresistance effect [22].

The crystal structure itself is also interesting, which can be seen in Fig. 1(a). The Au atoms, which have five neighbors each, have much larger atomic radii when compared with Mn, and so they form the framework that holds the structure together, with the Mn atoms fitting into the center of cubic Au cages throughout the lattice. Such an arrangement has implications for the electronic structure, which we will discuss later.

The common explanation for the $MnAu_2$ spiral is magnetic frustration, where $|J_1| < 4|J_2|$ [2,3]. In this notation, J_1 is the exchange between nearest-neighbor planes and J_2 is the exchange between second-nearest-neighbor planes. This interpretation was supported by density functional theory (DFT) calculations [23], in which the exchange constants were calculated using a relativistic extension [24] of the torque method [25] within the screened Korringa-Kohn-Rostoker formalism [26], and it was reported that $|J_1| < 4|J_2|$ was satisfied. However, the presence of highly itinerant carriers casts doubt on the idea of fully describing the magnetism in this system using a J_1-J_2 Heisenberg model. It is possible that the standard Heisenberg model can even fail to give a qualitative description of the magnetic state, as in the case of the Fe-based superconductors where such a description is dramatically inadequate; see Refs. [27,28]. Furthermore, while computational estimates for $J_{1,2}$ seem to satisfy the spiral criterion, direct calculations (not performed in Ref. [24]) show that the true DFT ground state is a uniform ferromagnet and not a spiral.

We are not aware of any other first-principles studies of the magnetic interactions and the ground state of $MnAu_2$. Overall, first-principles calculations of $MnAu_2$ have been sparse, aside from the above reference and a pair of reports with calculations of the density of states [29,30]. It is worth revisiting this problem using modern, full-potential DFT calculations with noncollinear spin configurations and extracting the exchange parameters from total-energy calculations, rather than by the torque perturbation theory with spherically symmetrized potentials [23]. Given that the Mn and Au states each correspond to distinct portions of the band structure, one may hope to elucidate microscopic reasons for the spiral ordering.

The paper is organized as follows. In Sec. II, we will detail our computational methods for calculating the electronic structure and total energy and extracting the exchange constants. We then follow, in Sec. III, with a report of our results and a subsequent discussion. Our main result is that, contrary to Ref. [23], a "vanilla" density functional theory does *not* account for the spirals in $MnAu_2$. However, upon accounting for on-site Coulomb correlations by applying a Hubbard U correction in the local spin-density approximation (LSDA) to the Mn d orbital, we see that spiral solutions appear for reasonable values of U and agree with the helical angle from experiment. This is an unexpected result, as the Hubbard U enhances localization and suppresses itinerant effects. Here, however, the correlated electrons forming local moments are different from the itinerant electrons mediating the magnetic interaction, and so a typical analysis using superexchange fails in such materials. Instead, the magnetism needs to be reanalyzed in a way similar to dilute magnetic semiconductors and Kondo lattices. We show, in particular, that the main effect of the application of U is to reduce hybridization between Mn bands and Au electrons forming the Fermi surface. While the nearest-neighbor superexchange is suppressed as $1/U$, the transferred RKKY-type interaction goes as $1/U^2$, introducing partial cancellation between the antiferromagnetic superexchange and ferromagnetic transferred interaction between the neighboring layer, which, in turn, enhances the $|J_2/J_1|$ ratio. We describe our conclusions in Sec. IV.

II. COMPUTATIONAL METHODS

We employed density functional theory (DFT) in three different implementations to study spin spirals in $MnAu_2$. We used projector augmented wave (PAW) potentials as implemented in VASP [31,32] and full-potential linear augmented plane waves as implemented in ELK [33] and WIEN2K [34]. The Perdew-Burke-Ernzerhof generalized gradient approximation (GGA) [35] was used for the exchange-correlation functional in all three codes and the local spin-density approximation (LSDA) [36] was also used in ELK. Correlation effects were considered in $MnAu_2$ using the DFT + U method in the fully localized limit [37], in which an empirical Hubbard U is introduced on the d orbitals of the Mn and/or Au atoms. Also, for a better comparison with the atomic sphere approximation (ASA) calculations of Ref. [23], which were not a full-potential treatment, we have performed selected calculations in the ASA using a linear muffin-tin orbitals (LMTO) code [38].

The material $MnAu_2$ belongs to the space group $I4/mmm$ with Wyckoff positions 2a for Mn and 4e for Au, which yields

planes of Mn and Au atoms (two layers of Au between each Mn layer). We set the lattice parameters to $a = 3.370\,13$ Å and $c = 8.758\,94$ Å and the internal parameter for Au to $z_{\mathrm{Au}} = 0.34$. The experimental ground state of $MnAu_2$ is a spin spiral, where ferromagnetic Mn planes (local moments are oriented in-plane) rotate about the c axis with a noncollinear pitch vector close to the incommensurate $\pi/2c$. To simulate the magnetic state, we consider spin spirals in $MnAu_2$ with two different methods. The first is to construct explicit spirals in supercells using noncollinear moments in the xy plane commensurate with $\mathbf{q} = \{0,0,\pi/2c\}$, see Fig. 1(b), which is done using the GGA functional in both VASP and ELK. The second approach is to use a spin-spiral method to simulate spirals in a primitive cell with one Mn atom, which is done using the LSDA functional in ELK alone.

We fit the energy calculations using the above methods to the one-dimensional Hamiltonian,

$$H = \mathrm{const} + \sum_i J_i \cos(i\theta), \tag{1}$$

where the sum is taken over the layers of Mn atoms. As this is a one-dimensional model, the exchange parameters J_i represent the coupling between entire *layers* of Mn atoms (the Mn layers can be seen in Fig. 1(b)) instead of the coupling between individual Mn atoms, i.e., J_1 is the coupling between two nearest-neighbor Mn layers, J_2 is the coupling between two next-nearest-neighbor Mn layers, and so on. Our primary interest is in the ratio $|J_2/J_1|$, so at a minimum we kept the first two terms in the sum with constants J_1 and J_2, and then we varied the number of layers in the sum to evaluate the robustness of the fit and the extracted parameters.

III. DISCUSSION

We calculated the band structure and density of states (DOS) of ferromagnetic $MnAu_2$ using the LSDA functional, shown in Figs. 2(a) and 3(a). The Mn d bands are fully spin split, corresponding to the ionic configuration of Mn(d^5) and the formal Mn valency of 5+. The total moment of the system is $3.93\mu_B$/Mn, and the reduction of the moment from the ideal $5\mu_B$ is due to the hybridization of Mn with Au. The experimental moment of $MnAu_2$ is $3.5\mu_B$ [19,22], and so the DFT result is about 9% larger in magnitude. The experimental moment is likely smaller than the DFT prediction because of zero-point fluctuations [39], which are not captured by DFT as it is a mean-field-type method. The bands crossing the Fermi energy consist of both Mn and Au character that is spin dependent: the minority bands have ∼1.6 times more Mn weight than the majority bands, while the majority bands have ∼1.5 times more Au weight than the minority bands. We note that while the Au bands are polarized at the Fermi energy, the net moment on the Au ions is zero.

The crystal structure of $MnAu_2$, as mentioned earlier, consists of Mn atoms placed in cubic Au cages. The band structure and DOS suggest that the electronic structure at the Fermi level is mostly determined by the Au atoms; therefore we calculated the band structure of a hypothetical Au system where the Mn atoms have been removed, shown in Fig. 2(b). In the real system there is a charge transfer of one electron per Au ion. We infer this from the band structure in Fig. 2(a) and

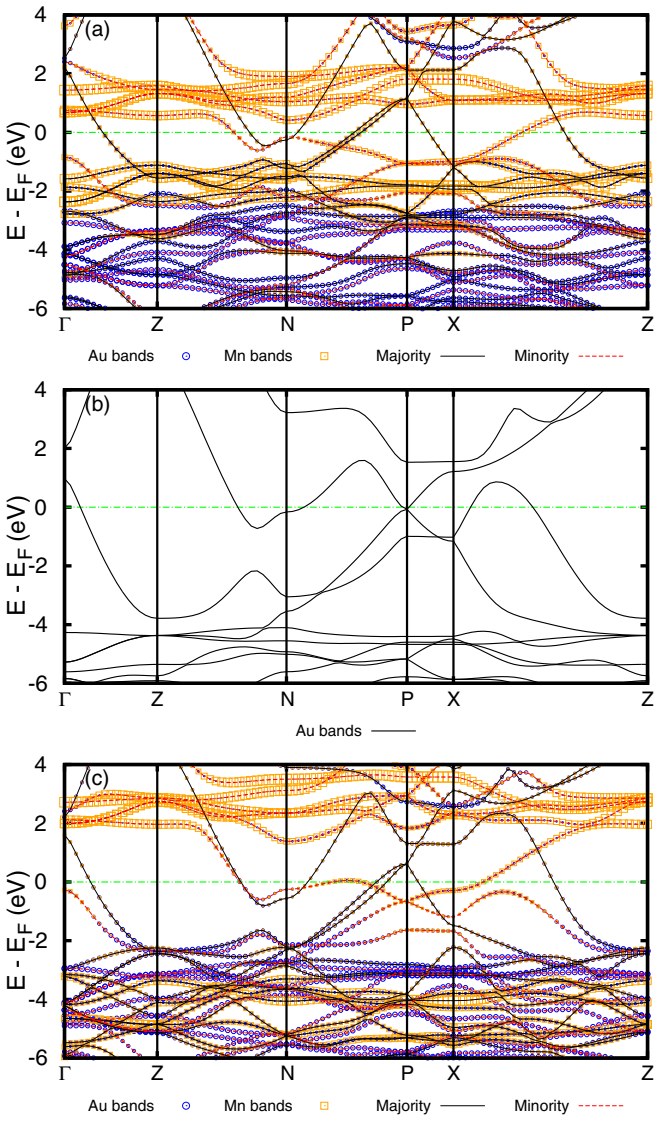

FIG. 2. (Color online) The spin- and species-resolved (see legend) band structure of $MnAu_2$ calculated using the FLAPW code ELK. The plot point size corresponds to the species weight. (a) The $MnAu_2$ band structure using the LSDA functional. (b) Hypothetical Au-only band structure with Mn atoms removed from the unit cell and Fermi level chosen to reflect Au^{1-} charge transfer. (c) The $MnAu_2$ band structure using the LSDA + U functional with $U = 4.7$ eV.

the density of states in Fig. 3(a), where we observe that the Mn 3d majority states are occupied and the Mn 3d minority states are unoccupied, which implies a Mn^{2+} charge state and so an electron is donated to each Au atom. Therefore the Fermi level of the hypothetical Au-only system is chosen to reflect an ionic charge of Au^{1-}. Comparing Figs. 2(a) and 2(b) shows the remarkable similarity between the two band structures, indicating that much of the electronic structure is due to the Au atoms only. The spin majority band crossing the Fermi energy in Fig. 2(a) is the same Au band in Fig. 2(b), while the spin minority band originates from the Mn atoms when they are placed into the structure, shifting the Au bands upwards in energy.

We next calculated the energy as a function of the spiral's helical angle θ using the spin-spiral method of ELK and

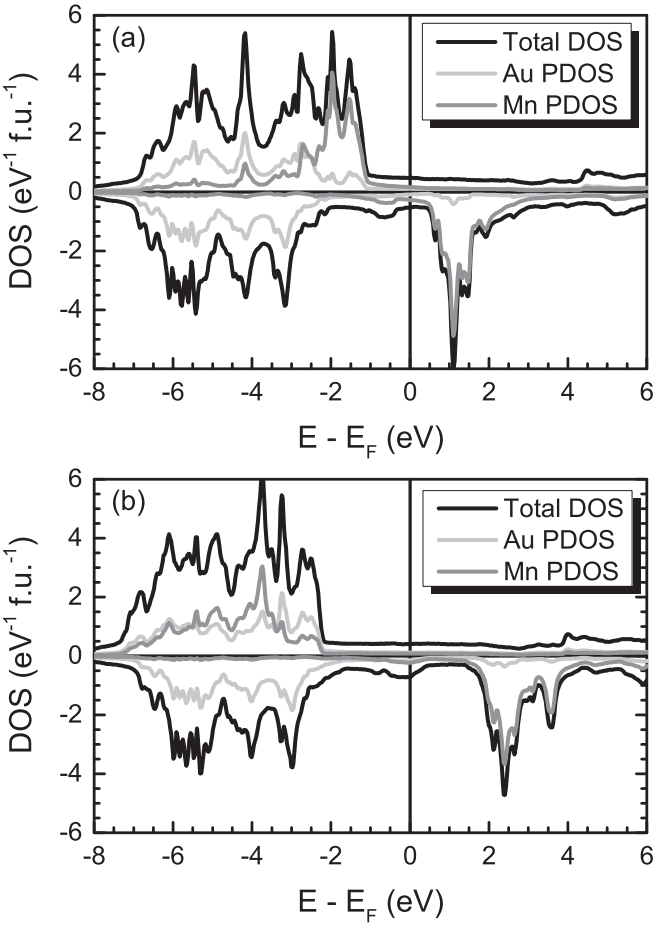

FIG. 3. The total and species-projected DOS of the ferromagnetic state of $MnAu_2$ calculated using the FLAPW code ELK. (a) The DOS using the LSDA functional. (b) The DOS using the LSDA + U functional with $U = 4.7$ eV.

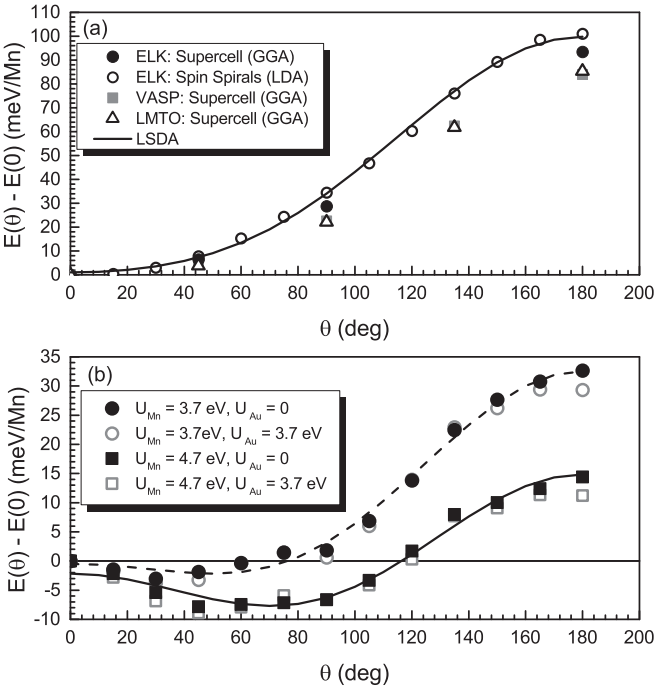

FIG. 4. The energy difference between a helical, in-plane spiral with angle θ and a ferromagnetic configuration in $MnAu_2$. (a) The energy dependence for LSDA and GGA functionals. The calculations are either spin-spiral calculations or explicit supercell calculations using VASP, ELK, or LMTO; see the legend. The solid line is the Eq. (1) fit to the ELK results. (b) The energy dependence using LSDA + U, where the Hubbard U is applied to Au and/or Mn d states. See the legend for the values of U. The dashed and solid lines are the Eq. (1) fits to the $U = 3.7$ eV and $U = 4.7$ eV calculations, respectively.

explicit spirals in supercells in both ELK and VASP. For the spin-spiral method, we used the LSDA functional [40], and for the supercell calculations, we used the GGA functional. We then computed the difference of $E(\theta) - E(0)$, comparing the energy of the spiral state with the energy of the ferromagnetic configuration. The results are summarized in Fig. 4(a). We consistently find in all cases that there is a preference for the ferromagnetic ground state. The qualitative trend across codes and functionals is the same. They differ with respect to the energy of the antiferromagnetic configuration, with the LSDA spiral method yielding the highest energy and the GGA VASP calculation yielding the lowest energy. Overall, this shows that DFT does not support a stable spin spiral, which is in disagreement with Korringa-Kohn-Rostoker (KKR) calculations from Ref. [23].

The origin of this disagreement cannot be ascribed to using different density functionals, as we found the same result with LSDA and GGA, nor in the approximations used to represent the crystal potential and electron (spin) density. We have verified, using a LMTO method that employs the same spherical approximation as the KKR method of Ref. [23], that the ground state is still ferromagnetic; see Fig. 4(a). An important difference may be that Ref. [23] uses the perturbative torque method to calculate the exchange constants, while we performed total-energy calculations for explicit spin-spiral configurations.

These results also hold when spin-orbit coupling (SOC) is turned on. The band structure of $MnAu_2$ with and without SOC is practically identical even though, in principle, Au is heavy enough to support non-negligible SOC effects. Importantly, the moment on Au is zero and therefore relativistic magnetic interactions of the DM type are excluded.

Although $MnAu_2$ is a good metal, the Mn d states are quite localized and are subject to local Hubbard correlations, not accounted for in straight DFT. It is well known that other compounds with Mn^{2+} require a Hubbard U on the order of 3–5 eV to reproduce the correct positions of Mn bands. With this in mind, we employed the LSDA + U method in combination with the spin-spiral calculations in ELK to incorporate additional electronic correlations. We applied the Hubbard U to the Mn $3d$ orbitals, using two plausible values for U: $U = 3.7$ eV and $U = 4.7$ eV. The parameter J was set to $J = 0.7$ eV. The Mn moment increased from its DFT value of $3.93\mu_B$ to $4.30\mu_B$ for $U = 3.7$ eV and $4.39\mu_B$ for $U = 4.7$ eV. This increase in the moment is due to the reduction in hybridization as the Mn $3d$ bands are moved away from the Fermi energy. In addition, we also checked if the application of $U = 3.7$ eV and $J = 0.7$ eV to the Au $5d$ orbitals affected the results. The results of these calculations

are shown in Fig. 4(b). We found that spirals form when U is applied to Mn states, while adding an additional U to Au had a negligible effect. For $U = 3.7$ eV, a shallow energy minimum of $\sim$3 meV appears around $\theta = 30^\circ$, and for a $U = 4.7$ eV, a deeper well of $\sim$8 meV/Mn appears around $\theta = 45^\circ$. Finally, we note that including U compresses the overall energy scale compared with the results of Fig. 4(a).

This evolution can be understood if we picture the relevant magnetic interaction as a combination of the nearest-neighbor-plane antiferromagnetic superexchange, proportional to $t_\perp^2/\Delta_{\uparrow\downarrow}$, and the transferred magnetic interaction mediated by the Au electrons. Note that $t_\perp$ is the effective interplane hopping and $\Delta_{\uparrow\downarrow}$ is the energy cost of transferring a Mn d electron to a neighboring site and flipping its spin. The transfer interaction can be visualized as the spin susceptibility of the Au subsystem multiplied by the square of the Mn-Au interaction vertex. In our case, this vertex is, to a first approximation, the Schrieffer-Wolff interaction [41,42], which is proportional to τ^2/Δ_{sd}, where τ is the Mn-Au hopping amplitude and Δ_{sd} measures how removed the occupied Mn d states are from the Fermi level. For a Fermi energy that falls roughly in the middle of the lower and upper Mn Hubbard bands, $\Delta_{sd} \approx \Delta_{\uparrow\downarrow}/2$. Furthermore, in the LSDA + U calculations, $\Delta_{\uparrow\downarrow} \approx \Delta_{\rm ex} + U$, where $\Delta_{\rm ex}$ is the LSDA (Stoner) exchange splitting.

The transferred interaction is distance dependent and is allowed to change sign, in contrast to the superexchange interaction. In particular, our calculations are consistent with a ferromagnetic nearest-neighbor interaction and an antiferromagnetic next-nearest-neighbor interaction. The next-nearest-neighbor exchange parameter is $J_1 \approx J_{\rm SE} + J^{(1)}_{\text{Mn-Au}}$, where $J^{(1)}_{\text{Mn-Au}} < 0$ and $|J_{\rm SE}| < |J^{(2)}_{\text{Mn-Au}}|$, while $J_2 \approx J^{(2)}_{\text{Mn-Au}}$, where $J^{(2)}_{\text{Mn-Au}} > 0$. Since $J_{\rm SE} \propto 1/\Delta_{\uparrow\downarrow}$ and $J_{\text{Mn-Au}} \propto 1/\Delta^2_{\uparrow\downarrow}$, as U increases both J_1 and J_2 shall decrease, but J_1 will decrease more rapidly as $J_{\rm SE}$ starts to play a more dominant role.

This is precisely what we observe in the calculations. Fitting to Eq. (1), we were able to reliably extract the constants J_1 and J_2, which remained robust regardless of the number of additional neighbors we included in the fit. The extracted constants are summarized in Table I along with the constants from Ref. [23], and the fits using the extracted constants are shown [43] in Fig. 4. In all cases, the J_1 parameter is ferromagnetic and J_2 is antiferromagnetic. Consistent with the argument above, the nearest-neighbor exchange J_1 is very sensitive to correlations, decreasing by a factor of $\sim$3 for $U = 3.7$ eV and $\sim$6 for $U = 4.7$ eV. In contrast, the decrease for J_2 is moderate for $U = 3.7$ eV and very small when U is increased further to $U = 4.7$ eV. Our LSDA value of J_2 is in good agreement with Ref. [23], while we find J_1 to be larger by a factor of 2.

TABLE I. The extracted exchange constants obtained by fitting the results of Fig. 4 to Eq. (1). For comparison, the calculated constants from Ref. [23] are also included. All constants are reported in units of meV.

		LSDA + U		LSDA
const	LSDA	$U = 3.7$ eV	$U = 4.7$ eV	Udvardi *et al.*
J_1	− 49.37	− 16.50	− 8.51	− 25.16
J_2	8.17	6.43	6.30	8.31

The band structure for $MnAu_2$ with $U = 4.7$ eV is shown in Fig. 2(c) and the DOS is in Fig. 3(b). As described, the primary effect of introducing U is to move the Mn d bands away from the Fermi level, which decreases the hybridization of Au with Mn, localizing Mn and decreasing the energy difference between ferromagnetic (FM) and layered antiferromagnetic (AFM) configurations. This, in turn, lowers the polarization of the Au bands, which mediate the transferred interaction, which then weakens the ferromagnetic exchange of J_1. We conclude that the spiral instability in $MnAu_2$ is driven by correlation effects which enhance the importance of the superexchange interaction relative to the transferred interaction induced by Au polarization.

Finally, we tried to identify the microscopic reason for the transferred interaction to change sign between $c/2$ and c along the c axis. A natural explanation would be in terms of a Fermi-surface nesting at an appropriate q_z. We note that q_z does not have to coincide exactly with the spiral wave vector; adding superexchange will shift it towards shorter wavelengths. Unfortunately, one cannot use the nonmagnetic $MnAu_2$ for investigating nesting effects, as the Mn moments are very large and a linear response treatment is not appropriate. The hypothetical $(Au^{1-})_2$ system is more appropriate due to the similarity of the band structures in Figs. 2(a) and 2(b), which become increasingly more alike with increasing U. To check for nesting, we calculated the noninteracting one-electron susceptibility for $(Au^{1-})_2$, defined as

$$\chi_0(\mathbf{q}) = \sum_{\alpha,\beta,\mathbf{k}} \frac{f(\epsilon_{\alpha,\mathbf{k}}) - f(\epsilon_{\beta,\mathbf{k}+\mathbf{q}})}{\epsilon_{\beta,\mathbf{k}+\mathbf{q}} - \epsilon_{\alpha,\mathbf{k}} + i\gamma}.$$

Note that this expression neglects any matrix elements arising from the fact that Au wave functions deviate from plane waves. We found a weak maximum at $\mathbf{q} = \{0,0,2\pi/c\}$, which would support antiferromagnetically aligned layers and would induce $J_1 > 0$ and $J_2 < 0$, opposite to what is needed for the experiment and what has been derived in Table I from the calculations. As it stands, further progress in understanding the Au-mediated transferred interaction requires calculations of the full spin susceptibility, which includes matrix elements and Stoner renormalization. At the present moment, we do not have the capability to perform these calculations.

IV. CONCLUSION

We have revisited the origin of spirals in $MnAu_2$ using accurate, full-potential, noncollinear DFT calculations, and found that contrary to previous findings, DFT alone is not sufficient to sustain a helical spiral state. We find that the spirals in $MnAu_2$ are supported by Hubbard correlations, which localize the Mn d electrons and strongly reduce the ferromagnetic coupling between neighboring Mn layers. This mechanism is in contrast to the common origin of spirals, which are typically due to relativistic effects such as the DM interaction or one-electron effects such as Fermi-surface nesting. This uncommon physical origin may be present in other materials where traditional explanations of spirals fail, such as FeAs.

ACKNOWLEDGMENTS

We are very grateful to Kay Dewhurst for his invaluable help and advice in setting up and performing spiral calculations in ELK. I.I.M. acknowledges funding from the U.S. Office of Naval Research (ONR) through the Naval Research Laboratory's Basic Research Program. J.K.G. acknowledges the support of the NRC program at NRL.

[1] A. J. P. Meyer and P. Taglang, J. Phys. Radium **17**, 457 (1956).
[2] U. Enz, J. Appl. Phys. **32**, S22 (1961).
[3] T. Nagamiya, K. Nagata, and Y. Kitano, Prog. Theor. Phys. **27**, 1253 (1962).
[4] T. Moriya, Phys. Rev. **120**, 91 (1960).
[5] I. Dzayloshinskii, J. Phys. Chem. Solids **4**, 241 (1958).
[6] J. Jensen and A. R. Mackintosh, *Rare Earth Magnetism* (Clarendon, Oxford, 1991).
[7] W. E. Evenson and S. H. Liu, Phys. Rev. Lett. **21**, 432 (1968).
[8] S. B. Dugdale, H. M. Fretwell, M. A. Alam, G. Kontrym-Sznajd, R. N. West, and S. Badrzadeh, Phys. Rev. Lett. **79**, 941 (1997).
[9] L. Nordström and A. Mavromaras, Europhys. Lett. **49**, 775 (2000).
[10] P. Bak and M. H. Jensen, J. Phys. C **13**, L881 (1980).
[11] O. Nakanishi, A. Yanase, A. Hasegawa, and M. Kataoka, Solid State Commun. **35**, 995 (1980).
[12] M. Kataoka and O. Nakanishi, J. Phys. Soc. Jpn. **50**, 3888 (1981).
[13] R. Plumier, J. Phys. (France) **27**, 213 (1966).
[14] J.-H. Chung, M. Matsuda, S.-H. Lee, K. Kakurai, H. Ueda, T. J. Sato, H. Takagi, K.-P. Hong, and S. Park, Phys. Rev. Lett. **95**, 247204 (2005).
[15] K. Selte, A. Kjekshus, and A. F. Andresen, Acta Chem. Scand. **26**, 3101 (1972).
[16] K. Segawa and Y. Ando, J. Phys. Soc. Jpn. **78**, 104720 (2009).
[17] D. Parker and I. I. Mazin, Phys. Rev. B **83**, 180403(R) (2011).
[18] A. Herpin, P. Mëriel, and J. Villain, Comptes Rendus **249**, 1334 (1959).
[19] A. Herpin and P. Mériel, J. Phys. Radium **22**, 337 (1961).
[20] Y. Nagata, T. Hagii, H. Samata, T. Uchida, S. Abe, C. F. Sung, and M. D. Lan, J. Alloys Compd. **284**, 47 (1999).
[21] K. Momma and F. Izumi, J. Appl. Crystallogr. **44**, 1272 (2011).
[22] H. Samata, N. Sekiguchi, A. Sawabe, Y. Nagata, T. Uchida, and M. D. Lan, J. Phys. Chem. Solids **59**, 377 (1998).
[23] L. Udvardi, S. Khmelevskyi, L. Szunyogh, P. Mohn, and P. Weinberger, Phys. Rev. B **73**, 104446 (2006).
[24] L. Udvardi, L. Szunyogh, K. Palotás, and P. Weinberger, Phys. Rev. B **68**, 104436 (2003).
[25] A. I. Liechtenstein, M. I. Katsnelson, V. P. Antropov, and V. A. Gubanov, J. Magn. Magn. Mater. **67**, 65 (1987).
[26] P. Weinberger and L. Szunyogh, Comput. Mater. Sci. **17**, 414 (2000).
[27] A. N. Yaresko, G.-Q. Liu, V. N. Antonov, and O. K. Andersen, Phys. Rev. B **79**, 144421 (2009).
[28] J. K. Glasbrenner, J. P. Velev, and I. I. Mazin, Phys. Rev. B **89**, 064509 (2014).
[29] L.-S. Hsu, Y.-K. Wang, and Y.-L. Tai, J. Alloys Compd. **416**, 11 (2006).
[30] L.-S. Hsu, T. Murakawa, H. Fujiwara, A. Sekiyama, S. Suga, S. Imada, M. Yano, T. Miyamachi, H. Higashimichi, J. Yamaguchi, G. Funabashi, M. Yabashi, T. Ishikawa, and A. Higashiya, J. Alloys Compd. **439**, 9 (2007).
[31] G. Kresse and J. Hafner, Phys. Rev. B **47**, 558(R) (1993).
[32] G. Kresse and J. Furthmüller, Phys. Rev. B **54**, 11169 (1996).
[33] Computer code ELK FP-LAPW, http://elk.sourceforge.net
[34] P. Blaha, K. Schwarz, G. K. H. Madsen, K. Kvasnicka, and J. Luitz, computer code WIEN2K (Karlheinz Schwarz, Techn. Universitat Wien, Austria, 2001).
[35] J. P. Perdew, K. Burke, and M. Ernzerhof, Phys. Rev. Lett. **77**, 3865 (1996).
[36] J. P. Perdew and Y. Wang, Phys. Rev. B **45**, 13244 (1992).
[37] A. I. Liechtenstein, V. I. Anisimov, and J. Zaanen, Phys. Rev. B **52**, R5467 (1995).
[38] O. K. Andersen, Phys. Rev. B **12**, 3060 (1975).
[39] The moment reduction due to zero-point fluctuations can be quite substantial in some cases, such as the Fe-based superconductors, where the DFT moment is $\sim 1.5-2.0\mu_B$ and the measured moment is $\sim 0.5-0.9\mu_B$. See I. I. Mazin and M. D. Johannes, Nat. Phys. **5**, 141 (2009).
[40] Our use of the LSDA functional over the GGA functional is a practical one. The spin-spiral algorithm in ELK works well with the LSDA functional, but there are numerical issues when the GGA functional is used. For example, with GGA, $\mathbf{q} = \{0,0,0\}$ and $\mathbf{q} = \{0,0,1\}$ yield different energies, even though they should be equivalent.
[41] J. Cibert and D. Scalbert, in *Spin Physics in Semiconductors*, Springer Series in Solid-State Sciences, edited by M. I. Dyakonov (Springer, Berlin, Heidelberg, 2008), Vol. 157, Chap. 13, pp. 389–431.
[42] D. Khomskii, *Basic Aspects of the Quantum Theory of Solids* (Cambridge University Press, Cambridge, 2010).
[43] The energies around $\theta = 0$ are not well described when only J_1 and J_2 are used for the LSDA + U ($U = 4.7$ eV) model fit. This can be improved by including additional neighbors in the Hamiltonian. What is important is that J_1 and J_2 are robust and do not change as more terms are included.